PSFC/JA-03-23

A Study of JET SOL Radial Transport Based on Particle Balance

Lipschultz, B., Andrew, P.[2], Coad, J.[2] Erents, K.[2], Felton, R.[2], Fundamenski, W.[2], Hidalgo, C.[3], Huber, A.[4], LaBombard, B., Matthews,G.[2], Mertens, P.[4], Pitts, R.A.[5], Silva, C.[6], Stamp, M.[2], Strachan, J.[7], Whyte, D.[8]

18 February 2004

[1]Plasma Science and Fusion Center, MIT, Cambridge, MA 02139 USA
[2]UKAEA, Culham, UK
[3]Asociación EURATOM-CIEMAT para Fusión, E-28040 Madrid, Spain
[4]KFA Research Centre 52425 Jülich, Germany
[5]CRPP EURATOM-Confédération Suisse, EPFL, 1015 Lausanne, Switzerland
[6]EURATOM/IST, Centro de Fusão Nuclear, 1049-001 Lisboa, Portugal
[7]PPPL Princeton NJ 08453 USA
[8]U. Wisc. Madison WI, USA

This work was supported by the U.S. Department of Energy, Cooperative Grant No. DE-FC02-99ER54512. Reproduction, translation, publication, use and disposal, in whole or in part, by or for the United States government is permitted.

Submitted for publication to *Nuclear Fusion.*

A Study of JET SOL Radial Transport Based on Particle Balance

B. Lipschultz[1]*, P. Andrew[2], J. Coad[2], K. Erents[2], R. Felton[2], W. Fundamenski[2], C. Hidalgo[3], A. Huber[4], B. LaBombard[1], G. Matthews[2], P. Mertens[4], R.A. Pitts[5], C. Silva[6], M. Stamp[2], J. Strachan[7], D. Whyte[8]

[1]MIT Plasma Science & Fusion Center, Cambridge Ma 02139, USA, [2]UKAEA, Culham UK, [3]Asociación EURATOM-CIEMAT para Fusión, E-28040 Madrid, Spain , [4]KFA Research Centre 52425 Jülich, Germany, [5]CRPP EURATOM-Confédération Suisse, EPFL, 1015 Lausanne, Switzerland, [6]EURATOM/IST, Centro de Fusão Nuclear, 1049-001 Lisboa, Portugal, [7]PPPL Princeton NJ 08453 USA, U. Wisc. Madison WI, USA

*This work supported by US Dept. of Energy under grant #DE-FC02-99ER54512

A. Introduction

Radial transport in a tokamak Scrape Off Layer (SOL) is important in determining a number of aspects of tokamak operation including recycling, impurity sources and transport, divertor dynamics, and potentially playing a role in the determining the density limit. This work represents an initial effort to apply an interpretive method [1] to JET plasmas to determine the underlying radial fluxes and transport in the outer SOL.

B. Experimental measurements

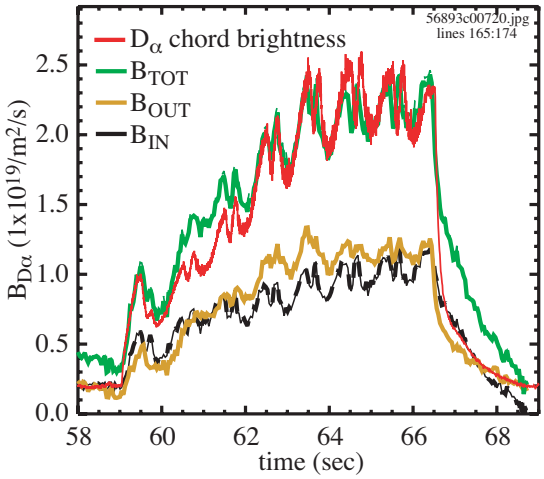

Figure 1: D_α chordal brightness (dah) used to calibrate the simulated camera D_α chord, B_{TOT}. Also shown are the contributions from the inner (B_{IN}) and outer edges (B_{OUT}) of the plasma.

A prerequisite to the radial transport analysis is to have a measure of the SOL profiles of n_e, T_e and the ionization source. S_{ION}. n_e and T_e are obtained in JET using the RCP scanning probe. We developed a measure of the ionization profile by digitizing a wide angle camera view of the main chamber ('KL1'). That provides us with an unnormalized brightness profile for visible emission across the midplane of the plasma. An emissivity profile is obtained through Abel inversion. A chordal integration along a major radius is then done to simulate the midplane D_α measurement view, 'dah'. A comparison of the simulated and 'real' chordal D_α measurements then determines the camera calibration, Figure 1. The Monte-Carlo neutral code, KN1D [2], using *only the plasma SOL n_e and T_e profiles and the midplane pressure,* has been utilised to model the same emissivity profiles. The modelled profiles match those derived from the wide-angle camera fairly well in both magnitude and general shape.

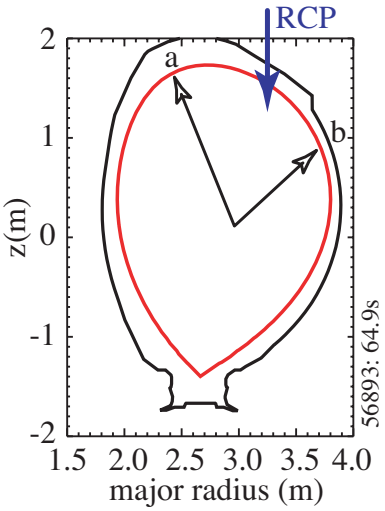

Figure 2: The separatrix is shown in red. The limiter shadow that the RCP samples is bounded at two points 'a' and 'b'.

The ion flux to the vessel surfaces outside the divertor serves as a boundary condition for the radial flux analysis. We derive the value for the radial flux at the limiter radius, $\Gamma_{\perp,i}$, from radial profile measurements of n_e and T_e and a model by LaBombard [3]. During the RCP sweep the probe samples plasma in the shadow of structures within the main chamber. Through field line mapping we were able to delineate the outline of this shadow region. As illustrated in Figure 2 this 'window frame' through which the radial flux passes, is bounded poloidally by a toroidal ring of tiles at the top of the machine and the poloidal limiters at the outer midplane. Given that $S_{ION} < \nabla\cdot\Gamma$ in the limiter shadow, the radial ion flux is then $\Gamma_{\perp,\mathrm{lim}} = \dfrac{2\cdot\Gamma_{\parallel,0}\cdot\lambda_n}{L_\parallel} = \dfrac{2\cdot n_{\mathrm{lim},0}\cdot c_s\cdot\lambda_n}{\pi\cdot R\cdot q}$ where $n_{lim,0}$ is the density at the limiter radius. The typical values for the JET limiter shadow are $\lambda_n \sim 14$ mm, $T_e \sim 10$ eV, ~ 2.9 m, $q \sim 3.5$. This gives $\Gamma_{\perp,i} \sim 28 x n_{lim,0}$ (m^{-3}). The following table summarizes the radial ion flux reaching the limiters radius for the time slices studied. The inward neutral flux, $\Gamma_{0.\perp}$, determined from the midplane pressure is shown as well.

Shot	Time	$\bar{n}_e$(m^{-3})	n_{lim} (m-3)	$\Gamma_{i.\perp}$ (m^{-2}/s)	$P_{midplane}$ (mT/Pa)	$\Gamma_{0.\perp}$ (m^{-2}/s)
56836	60.52	$1.2x10^{19}$	$2.5x10^{17}$	$7x10^{18}$	.0042/.00055	$2x10^{19}$
56836	62.53	$1.2x10^{19}$	$2.5x10^{17}$	$7x10^{18}$	.0044/.00058	$2.1x10^{19}$
56836	66	$1.9x10^{19}$	$8x10^{17}$	$2.24x10^{19}$	.0086/.0011	$4.1x10^{19}$
56836	68	$2.3x10^{19}$	$1x10^{18}$	$2.8x10^{19}$	.021/.028	$1.x10^{20}$
56893	58.24	$1.5x10^{19}$	$1x10^{17}$	$2.8x10^{18}$	.0035/.00046	$1.2x10^{19}$
56893	60.24	$2.5x10^{19}$	$1.5x10^{17}$	$4.2x10^{18}$	.008/.001	$3.8x10^{19}$
56893	62.22	$3.4x10^{19}$	$8x10^{17}$	$2.24x10^{19}$	.015/.002	$7.1x10^{19}$
56893	64.23	$3.7x10^{19}$	$1.2x10^{18}$	$3.4x10^{19}$	.022/.029	$1.x10^{20}$

All fluxes increase with increasing $\bar{n}_e$. We see that $\Gamma_{\perp,i} \sim \Gamma_{0.\perp}/3$. It appears that the ion flux to the chamber surfaces, although substantial, does not account for all of the midplane neutrals (pressure). The remaining neutrals could then come from divertor leakage.

C. Radial flux analysis

We can expand our analysis of radial fluxes to all points in the SOL. The derivation of the underlying radial transport is based on particle balance between ionisation source and parallel and perpendicular particle losses [1,4]. We start with the basic continuity equation for quantities averaged over the SOL:

$$\nabla_\perp\cdot\Gamma_\perp + \nabla_\parallel\cdot\Gamma_\parallel = S_{ION} \tag{1}$$

$$\Gamma_\perp(r) = \int_{sep}^{r}\left[S_{ION}(r) - Mn(r)c_s(r)/L_\parallel\right]\cdot dr + \Gamma_{\perp,sep} \tag{2}$$

$$\Gamma_{\perp,sep} = \int_{0}^{sep}\left[S_{ION}(r)\right]\cdot dr + f_c\int_{sep}^{wall}\left[Mn(r)c_s(r)/L_\parallel\right]\cdot dr \tag{3}$$

$$\Gamma_{\perp,wall} = \int_{0}^{wall}\left[S_{ION}(r)\right]\cdot dr - (1-f_c)M\int_{sep}^{wall}\left[n(r)c_s(r)/L_\parallel\right]\cdot dr \tag{4}$$

where M is Mach number, $c_s \sim (kT_e/m_i)^{1/2}$ is sound speed, $L_{//}$ is the field line length between divertors, S_{ION} is the volumetric ionization source rate. f_c is the fraction of ion flux *into* the divertor that recycles and enters the core. The divertor leakage flux fraction is then $(1-f_c)$. The boundary condition for this analysis is the wall flux measurement of the previous

section. We assume a Mach profile based on measurements [4-8] that is 0.2 at the separatrix rising rapidly to M=0.4 at r-r_{sep}=17 mm, constant for greater r-r_{sep}. The value of f_c assumed was 0.9. However, it has little effect on the analysis once the $\Gamma_{\perp,wall}$ is known [4]. Figure 3 shows the plasma profiles input to this analysis (a-c) as well as the radial ion flux (d). The effective transport coefficients are derived assuming diffusive (e) - $\Gamma_\perp(r) = -D_{eff}\nabla n(r)$, or convective (f) - $\Gamma_\perp(r) = n(r)v_{eff}(r)$ transport. The radial ion flux, $\Gamma_\perp$, is constant or dropping across the SOL. D_{eff} and v_{eff} both increase with distance from the separatrix. The values of D_{eff} and v_{eff} do not seem affected by changing plasma conditions.

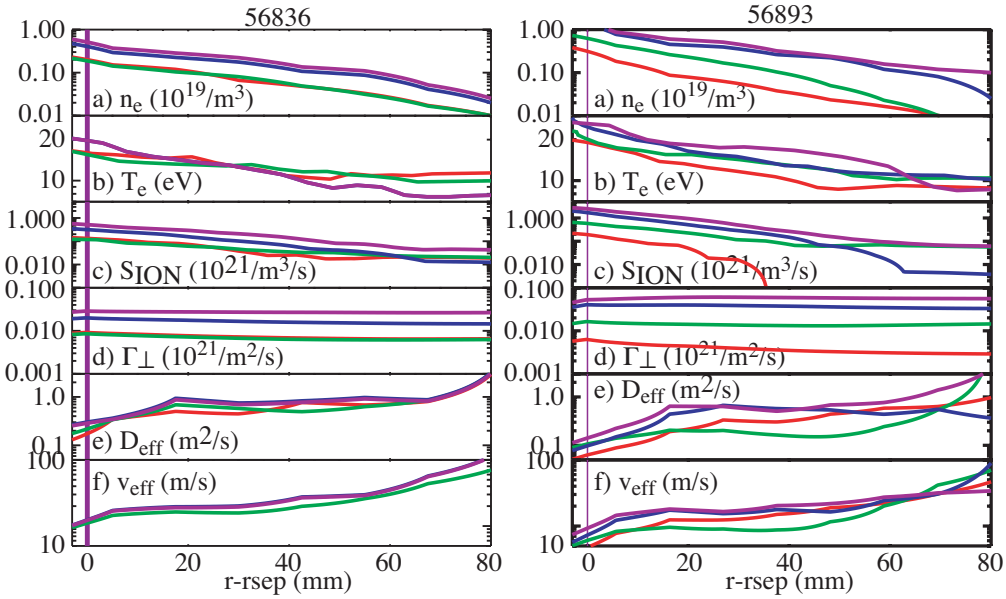

Figure 3: Radial transport analysis for a set of 8 time slices over two shots – 56836 (I_p=1MA, B_T=1T) and 56893 (I_p=2MA, B_T=2T), described in the above table.

C. Dimensionless scaling analysis

The radial flux analysis shown in figure 3 shows little or no variation in the inferred transport coefficients even though the SOL characteristics have changed considerably. We use a dimensionless similarity scaling approach [9-10] as a vehicle to discuss the role of

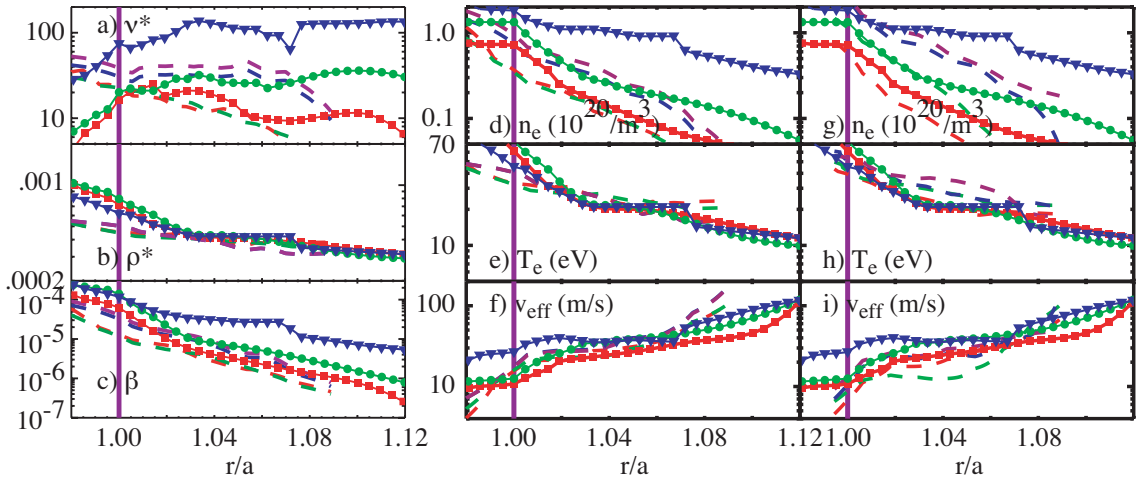

Figure 4: Dimensionless scaling comparison of JET and Alcator C-Mod. The JET data are dashed lines. The C-Mod data are solid lines + symbols. Dimensionless parameters for the JET (56836) and C-Mod discharges shown in a-c. JET and C-Mod SOL parameters are shown in 4d-f (56836) and 4g-i (56893).

plasma and atomic physics. The profiles of ν^*, ρ^*, and β are shown in figure 4a-c for the one JET shot already discussed (56836, dashed lines) as well as for three density cases from Alcator C-Mod (1 MA, 5.3 T). The Alcator C-Mod and JET (56836) shots have dimensionlessly similar SOLs. Note also the ν^* and β variation within a shot as the density is varied,.

We can use the dimensionless scaling to directly compare the JET SOL characteristics with that from C-Mod, Figure 4d-i. The n_e profiles show some similarity, shorter e-folding lengths in the 'near' SOL ($1.< r/a < 1.02$) than in the SOL 'far' from the separatrix. The dimensionless scaling between C-Mod and JET appears to predict the v_{eff} profile to within a factor of 2. The JET shot at higher toroidal field (56893, 4g-i) has lower ρ^* and β. But this substantial change only lowers v_{eff} slightly compared to 56836.

But what of the role of neutrals? The mean free path for neutrals (ionization + CX), when normalized by the machine size, $\lambda_{0,mfp}/a$, should scale as a. Thus the JET SOL should be much more transparent to neutrals than C-Mod. Since the transport is so similar on the two experiments we believe that the difference in profile shapes (generally flatter on C-Mod, Fig. 4) is due to a radial 'high-recycling' condition whereby the neutral pressure, and ionization in the far SOL, must be much higher in C-Mod due to the poor probability of their reaching the core plasma.

D. Summary

The JET SOL profiles evidence some of the same characteristics of other tokamaks. There are 'near' and 'far' SOL regions with short and long e-folding lengths. The 'far' SOL n_e profile flattens with increasing density. The flattening is less pronounced in JET.

Radial transport analysis using particle balance has been done. It shows that the radial ion flux is dropping slowly or flat across the SOL. The effective transport coefficients, D_{eff} and v_{eff}, both increase across the SOL by factors of 2-10. D_{eff} and v_{eff}, are similar to that found for C-Mod and DIII-D.

Dimensionless scaling analysis indicates that ν^*, ρ^*, and β are not strong factors controlling the transport. The dimensionless scaling from JET to C-Mod works well. Neutrals do not appear to play a role in setting the transport coefficients- large changes in neutral midplane densities do not correlate with changes in v_{eff} or D_{eff}. However, shorter normalized neutral mean free path, $\lambda_{0,mfp}/a$ does correlate with flattening of n_e profile.

References

[1] LaBombard, B., et al., Phys. Plasmas 8 (2001) 2107.
[2] LaBombard, B. MIT report PSFC-RR-01-03.
[3] LaBombard, B., et al., Nucl. Fusion 40 (2000) 2041.
[4] Lipschultz, B., et al, 'Comparison of ion transport in the Scrapeoff Layer plasmas of Alcator C-Mod and DIII-D', to be submitted to PPCF.
[5] LaBombard, B., et al., J. Nucl. Mater. 241-243 (1997) 149.
[6] deKock. L., et al., 1989 Proc. 12th Int'l Cong. on Plasma Phys. & Contr. Nucl. Fs. Res. vol 1 (IAEA) 467.
[7] Loarte, A., 1993 Proc. 20th European Conf. on Contr. Fus. & Plasma Phys. vol 17C (Lisboa) 555.
[8] Asakura, N., Plasma Phys. & Control. Fusion 44 (2002) 2101.
[9] Connor, J.W., Taylor, J.B., Nucl. Fusion 17 (1977) 2047.
[10] Kadomtsev, B.B., Sov. J. Plasma Phys. 1 (1975) 295.